Available online at www.sciencedirect.com
ScienceDirect
Polymer 48 (2007) 5125–5132
polymer
www.elsevier.com/locate/polymer

Uniaxial deformation of overstretched polyethylene: In-situ synchrotron small angle X-ray scattering study

Yujing Tang [a], Zhiyong Jiang [a], Yongfeng Men [a,*], Lijia An [a], Hans-Friedrich Enderle [b], Dieter Lilge [b], Stephan V. Roth [c], Rainer Gehrke [c], Jens Rieger [d]

[a] *State Key Laboratory of Polymer Physics and Chemistry, Changchun Institute of Applied Chemistry, Chinese Academy of Sciences, Graduate School of Chinese Academy of Sciences, Renmin Street 5625, 130022 Changchun, PR China*
[b] *Basell Polyolefine GmbH, R&D, 65926 Frankfurt, Germany*
[c] *HASYLAB am DESY, Notkestr. 85, 22607 Hamburg, Germany*
[d] *BASF Aktiengesellschaft, Polymer Physics, 67056 Ludwigshafen, Germany*

Received 8 March 2007; received in revised form 24 May 2007; accepted 20 June 2007
Available online 28 June 2007

Abstract

Synchrotron small angle X-ray scattering was used to study the deformation mechanism of high-density polyethylene that was stretched beyond the natural draw ratio. New insight into the cooperative deformational behavior being mediated via slippage of micro-fibrils was gained. The scattering data confirm on the one hand the model proposed by Peterlin on the static structure of oriented polyethylene being composed of oriented fibrils, which are built by bundles of micro-fibrils. On the other hand it was found that deformation is mediated by the slippage of the micro-fibrils and not the slippage of the fibrils. In the micro-fibrils, the polymer chains are highly oriented both in the crystalline and in the amorphous regions. When stretching beyond the natural draw ratio mainly slippage of micro-fibrils past each other takes place. The thickness of the interlamellar amorphous layers increases only slightly. The coupling force between micro-fibrils increases during stretching due to inter-microfibrillar polymer segments being stretched taut thus increasingly impeding further sliding of the micro-fibrils leading finally to slippage of the fibrils.

Keywords: SAXS; Oriented polyethylene; Deformation

1. Introduction

Polyethylene (PE) is widely used in pipe applications for gas, water and oil transportation because of it's excellent crack-resistance. Despite of many investigations on the crack growth mechanism in PE there are still discussions about the factors that control the crack speed [1–7]. There is agreement that near a crack tip there is always a craze structure consisting of highly stretched fibrils connecting the crack surfaces. The propagation of the crack is therefore accompanied by the breakdown of craze fibrils. It is thus important to gain knowledge about the deformation mechanism of these fibrillar structures under tension. It has been shown that the fibres form by transformation of the original spherulitic structure of the solid PE when the material is deformed to it's natural drawn ratio [8–11]. Peterlin [12] and Ward et al. [13] suggested a model of the fibre structure where the fibre is composed of fibrils being built up by stacks of crystalline lamellae whose normal is parallel to the direction of stretching. These stacks of lamellae are called micro-fibrils in the following. The crystalline lamellae are embedded in an amorphous network. Peterlin [12] proposed that – upon stretching the fibre – the fibrils slip past each other since it seems to be easier to overcome the opposing forces imposed by chains connecting adjacent fibrils than separating more strongly connected micro-fibrils or pulling apart lamellae that are connected by a dense network of amorphous chains.

* Corresponding author. Tel.: +86 431 85262907; fax: +86 431 85262954.
E-mail address: men@ciac.jl.cn (Y. Men).

0032-3861/$ - see front matter © 2007 Elsevier Ltd. All rights reserved.
doi:10.1016/j.polymer.2007.06.056

In this work, we investigate the deformational process of a broadly distributed high-density polyethylene (HDPE) [14] that was pre-stretched to it's natural draw ratio by means of the synchrotron small angle X-ray scattering (SAXS) technique. The SAXS data confirm that the fibre structure of the oriented HDPE is similar to the one proposed by Peterlin. But it is found that the deformation mechanism differs qualitatively from the one proposed by Peterlin. Possibly due to the special composition of the broadly distributed HDPE, one observes that during tensile deformation of the pre-stretched sample the slippage of micro-fibrils occurs earlier than that of fibrils indicating a stronger interaction between the fibrils than between the micro-fibrils.

2. Experimental section

2.1. Materials

The HDPE used in this study was supplied by BASELL Polyolefine GmbH, Frankfurt, Germany. The molecular weights are $M_w = 3.7 \times 10^5$ g/mol and $M_n = 7.8 \times 10^3$ g/mol. The material is broadly distributed and is composed of linear short chains and long chains with short side chain branches [14] and is typically used for pipe applications. The material was first compression molded at 180 °C. Solidification then occurred during quenching the melt into ice water yielding a plate of 2 mm thickness. A rectangular strip of 20×70 mm^2 was cut from the plate. The strip was first stretched at room temperature such that the neck propagated at a constant crosshead speed of 10 mm/min. The strain (ε_H) at the natural draw ratio for this sample was 1.32 where ε_H denotes the Hencky measure of strain and is defined as

$$\varepsilon_H = 2\ln\frac{b_0}{b} \tag{1}$$

where b_0 and b are the widths of sample before and after deformation. Here, the width instead of the length of the sample was used to deduce the Hencky measure of strain because the sample deforms inhomogenously and thus only local true strain can be determined. The advantage of using the Hencky measure of strain is it's additivity when the deformation is accomplished jump-wise as in this work [15]. The necked part of the sample was cut out for further online stretching measurements. The crystallinities of the sample before and after necking, determined by differential scanning calorimetry experiments, are 64% and 61%, respectively.

2.2. Small angle X-ray scattering

Synchrotron SAXS measurements were performed at the synchrotron beamline BW4 at HASYLAB, DESY, Hamburg, Germany. The energy of the X-ray radiation was 8.979 keV, resulting in a wavelength of 0.13808 nm. The pre-stretched sample was mounted onto a portable tensile tester (Kammrath and Weiss GmbH, Germany) at the beamline. The distance between the sample and the detector was 3938 mm. At this distance the effective scattering vector q ($q = 4\pi\sin\theta/\lambda$, where 2θ is the scattering angle and λ the wavelength) lies in the range 0.03–0.8 nm^{-1}. The SAXS patterns were recorded with a two-dimensional MarCCD detector with an active area of 16 cm diameter (2048×2048 pixels, pixel size 79.1 μm). Data processing was performed with the computer program "Fit2D" [16]. The SAXS patterns were normalized to the primary beam intensity and corrected for background scattering. Changes in scattering intensities due to varying sample thicknesses have been corrected by measuring sample adsorption using ionization chambers before and after the sample and performing the respective data correction. The pre-stretched sample was stretched at a crosshead speed of 16.2 μm/s to a pre-set elongation. The SAXS patterns were recorded within 2 min before further stretching.

3. Results and discussion

Fig. 1 shows SAXS patterns of the pre-stretched HDPE at different strains. The two maxima occurring along the stretching direction on both sides of the beam stop are due to the scattering from the oriented lamellar structure in the micro-fibrils. The equatorial streaks across the beam stop indicate the existence of fibrils [17]. All SAXS patterns indicate a high degree of orientation of the lamellae and the existence of fibrils. The scattering patterns coincide with the one derived from the fibril model proposed by Peterlin and modified by Murthy et al. [17]: cf. Fig. 2. In this model, an oriented polyethylene sample contains a fibrillar structure made up of fibrils. The modification of Murthy et al. consists in the assumption that the fibrils do not occur as neat bundles but they are packed in a disordered jammed state. The fibrils consist of micro-fibrils, i.e. stacks of lamellae with their normal parallel to the stretching direction. It must be mentioned that although we introduced micro-fibrils in the model corresponding to the ones proposed by Peterlin, prior to a detailed SAXS data analysis it is not possible to prove the existence of micro-fibrils.

The scattering vectors along and perpendicular to the stretching direction are defined as q_1 and q_2, respectively. The strain of the pre-stretched HDPE is 1.32. For an easier discussion in the following we set this strain value to zero. Further stretching finally yields a strain of 0.48.

In order to obtain more detailed information, the structural parameters of lamellae and fibrils are discussed separately in the following. From the SAXS data measured along the meridian two parameters to describe the lamellar structure are derived, namely, the long spacing d_{ac} ($d_{ac} = d_a + d_c$, where d_a and d_c are the average thickness of the amorphous and the crystalline layers, respectively) and the lateral dimension of the lamellae. We did not consider tilting of the crystalline lamellae with respect to the fibre axis since no sufficient evidence for four-point scattering patterns was observed.

The long spacing of stacks of lamellae along the stretching direction can be obtained by considering the scattering intensity distribution along the q_1 direction $I(q_1)$, which was obtained by meridian scans along q_1 for certain intervals of q_2 as schematically shown in the top left corner of Fig. 3. The profiles of $I(q_1)$ of a sample stretched at different strains are

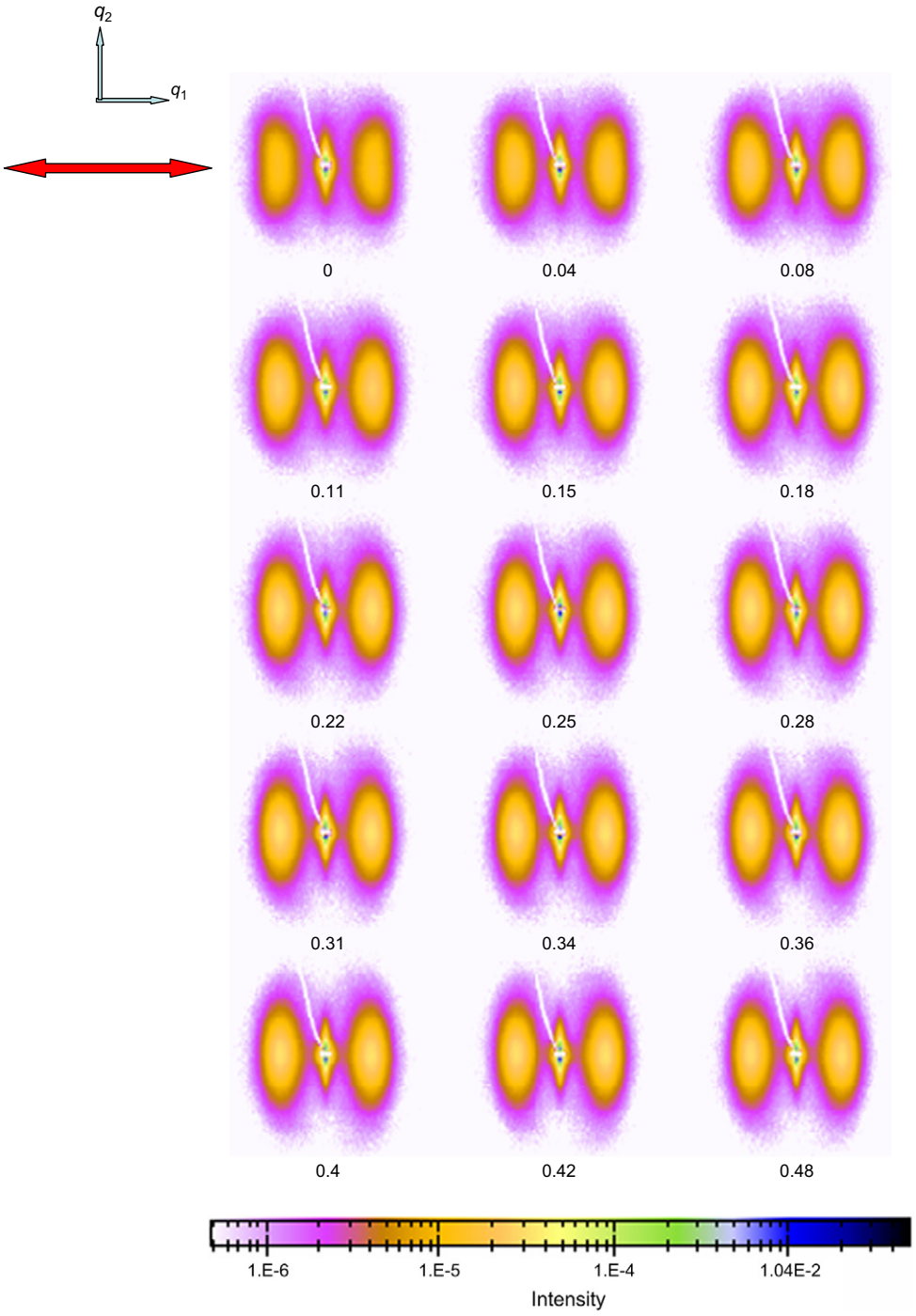

Fig. 1. Small angle X-ray scattering patterns of drawn pre-stretched HDPE at different macroscopic strains. The red arrow indicates the drawing direction.

shown in Fig. 3. The long spacing, d_{ac} measured along q_1, of the samples was obtained from the peak position of $I(q_1)$ according to Bragg's law:

$$d_{ac} = \frac{2\pi}{q_{1,max}} \tag{2}$$

It is seen that the peak position of $I(q_1)$ moves to smaller q values with increasing strain implying that the long spacing d_{ac} increases slightly with strain. The average thickness of the amorphous and crystalline regions along the meridianal direction can be derived from the one-dimensional correlation function of the distribution of the electron density in the lamellar stacks $K(z)$ as follows [18–21]:

$$K(z) = \frac{\int_0^\infty I(q_1)\cos(q_1 z)\mathrm{d}q_1}{\int_0^\infty I(q_1)\mathrm{d}q_1} \tag{3}$$

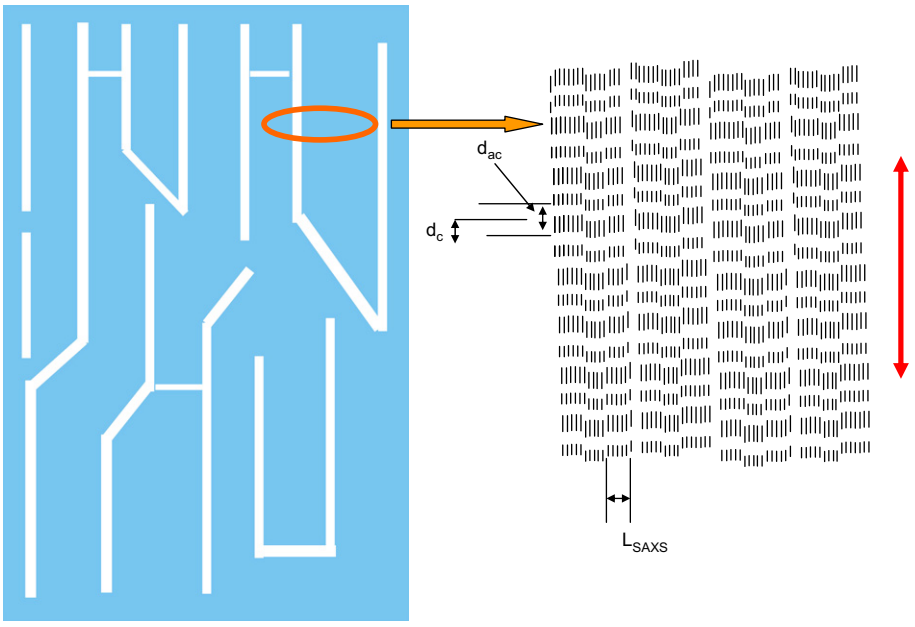

Fig. 2. A hybrid model based on ideas of Peterlin and Murthy to interpret the SAXS data. L_{SAXS} is the lamellar lateral size, d_{ac} is the lamellar long spacing, d_c is the lamellar thickness. The red arrow indicates the stretching direction (modified Murthy's model, Fig. 4 in [17]).

where z is the drawing direction. The Lorentz correction where $I(q_1)$ is multiplied by q_1^2 is not applied because of the anisotropic orientation of the lamellae in the sample [18,21,22].

The plot in the lower part of Fig. 3 shows the one-dimensional correlation function of density along q_1. The inset in Fig. 3 shows how the average thickness of the amorphous layer (d_a) and of the long spacing (d_{ac}) are derived. Because the sample used in the present study was a high-density polyethylene with a typical crystallinity above 60 wt%, one can assign the small value to the average thickness of the amorphous layers. The average thickness of the crystalline layers is then given by the relation $d_c = d_{ac} - d_a$. Of particular interest is the comparison of the crystallinity values derived from DSC and SAXS measurements. Having the thicknesses of long spacing and crystalline lamellae one can define a linear crystallinity ($\alpha_{c,l} = \frac{d_c}{d_{ac}}$). Our SAXS data at necked region of the sample yields a linear crystallinity of 66% being slightly larger than the one derived from DSC measurement. This small deviation can be explained as follows: DSC experiments measure overall crystallinity within the whole sample whereas SAXS peak position only presents structural details within certain correlated stacks indicating the crystallinity within the stacks only. Slightly larger value of SAXS crystallinity than that of DSC also indicates the existence of the inter-fibrillar disordered regions.

Fig. 4 shows the long spacing (d_{ac}), the lamellar thickness (d_c) and the amorphous thickness (d_a) and their relative changes (microscopic strains) as a function of the macroscopic strain. The data indicate that the increase of long spacing is mostly due to the increase of amorphous layer thickness. At very small strains of less than 0.05, the average thickness of the amorphous layers follows affine deformation behavior with respect to the macroscopic strain. When the macroscopic strain exceeds a value of 0.05, the deformation of the amorphous layers, of the lamellae as well as of the long spacing does no longer follow the macroscopic strain. This result implies that there must be some other mechanism to allow for the macroscopic strain.

The SAXS peaks discussed so far with respect to their meridian behavior exhibit a pronounced broadening in the equatorial direction. Such a broadening might be either due to misalignment of the lamellar structures with respect to the stretching direction or due to the limited lateral dimension of the lamellae making up the stacks – or to both. At first sight there seems to be no indication for a four-point scattering pattern typical for samples with misaligned stacks of lamellae, therefore it was initially assumed that the equatorial broadening is caused by the small lateral size of the lamellae. This lateral size can be derived from the width Δq_2 of the peaks at half height in the equatorial direction according to

$$L_{SAXS} = \frac{2\pi}{\Delta q_2} \tag{4}$$

By evaluating the data it was found that the resulting lamellar dimensions increased with increasing strain (data not shown here). This behavior represents an unlikely physical scenario since it is not to be expected that the crystals grow laterally upon stretching, rather the opposite behavior is to be expected, i.e. breakage due to micro-fibril slippage, see below. For this reason in a second approach it was assumed that lamellar misalignment is responsible for the peak broadening indeed. Fig. 5 shows azimuthal scans of the lamellar peaks along q_2 at different macroscopic strains. The tilting angle of stacks of lamellae with respect to the fibre axis and the average lateral dimension of the lamellae are obtained from the profiles of the intensity distribution along the straight line, $I(q_2)$. The

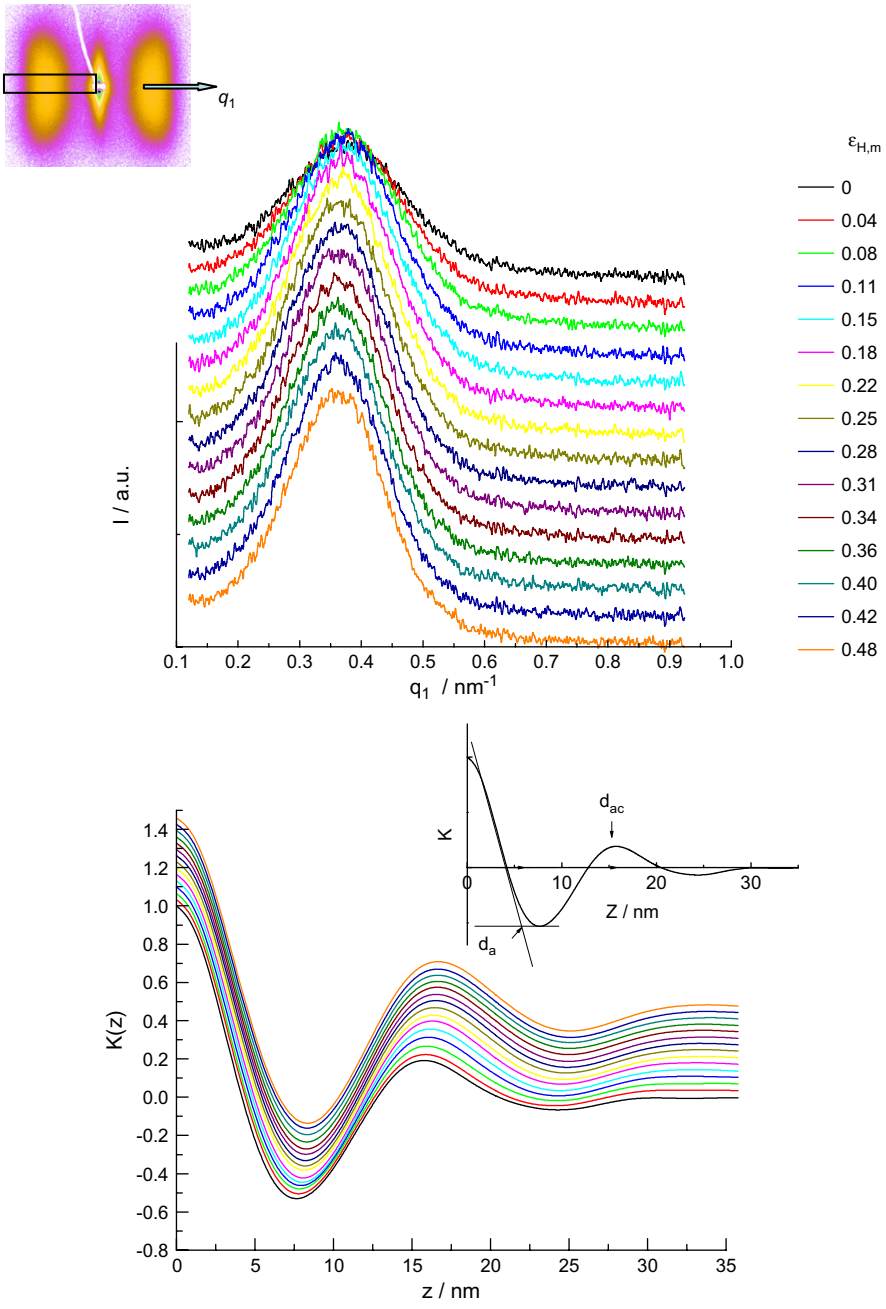

Fig. 3. SAXS: one-dimensional scattering intensity distribution along the stretching direction (top) and it's correlation function (bottom). Curves were shifted vertically for sake of clarity. The maximum position in the top curves indicates the long spacing (d_{ac}) of the lamellar stacks. The long spacing (d_{ac}) and the average amorphous thickness (d_a) can be obtained from the correlation function as shown in the inset of the bottom figure.

curves of $I(q_2)$ were fitted with two Lorentz functions as shown in the inset of Fig. 5. The width of the resulting Lorentz function (Δq_2) is related to the lateral size of the crystalline lamellae and the separation of the centers of the two Lorentz functions ($\Delta\chi$) is assigned to the stack tilting [18,23]. The lateral size of the lamellae was obtained according to Eq. (4). It must be mentioned that the use of this method is only valid when the orientation is perfect. Here, for sake of simplicity, we assume a perfect orientation of the crystalline lamellae. The tilting angle (Φ) between the normal of lamellae and the fibre axis was obtained with the following equation:

$$\Phi = \tan^{-1}\frac{\Delta\chi}{2q_{1,\max}} \tag{5}$$

where $q_{1,\max}$ is the lamellar peak position along q_1 at $q_2 = 0$. The tilting angle and lateral size of the lamellae vary with the macroscopic strain as shown in Fig. 6. The data in Fig. 6 indicate that stretching leads to a less tilted state of the lamellae stacks and an apparently slightly larger lateral size of lamellae. The slight change in the lateral size of the lamellae as a function of strain is not further considered here since it lies within the limits of the fitting error. When

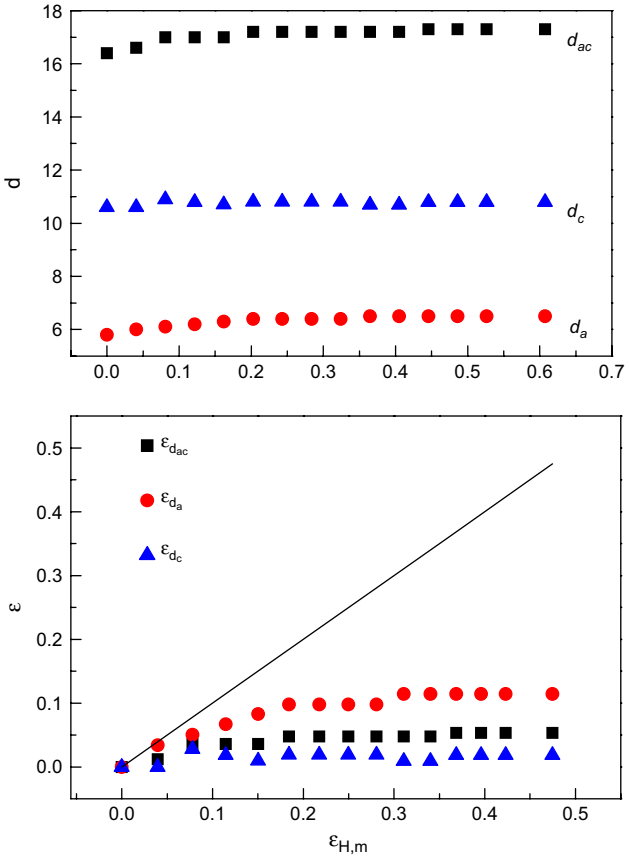

Fig. 4. The long spacing (d_{ac}), lamellar thickness (d_c) and the amorphous thickness (d_a) (top) and their strains (bottom) as function of macroscopic strain. The straight line in the bottom figure represents the affine deformation behavior.

being stretched, the normal of the lamellae moves toward the stretching direction gradually. The initial slight misalignment of the stacks of lamellae is assumed to be due to the relaxation of the sample which occurs when the sample is stretched to it's natural draw ratio and then released. Because of entropic reasons stacks of lamellae will reorient locally to a certain extent after this release.

Before discussing the length of the fibrils, we try to estimate the width of the fibrils using the Guinier approximation by considering the intensity distribution along the equatorial streak ($I = I_0 \exp(-q_2^2 R^2/3)$) [17,24,25]. The value of R denotes the radius of gyration of the fibrils in their lateral direction. The calculation yields a value of about 45 nm. It must be mentioned that the Guinier approximation is strictly applicable for monodisperse systems only when $qR < 1$. This condition is not fulfilled in our case where $q_{\min} = 0.05\ \mathrm{nm}^{-1}$. But experience indicates that the use of this formalism gives at least a rough estimate of the respective dimension under the given conditions. This R value is significantly larger than the lateral size of lamellae (15 nm). The data thus confirm that fibrils must contain bundles of micro-fibrils as proposed by Peterlin. Micro-fibrils are considered to be stacks of lamellae and thus to have similar width as the lateral size of lamellae.

The length of fibrils was estimated by Ruland's method [26,27]. The streak scattering across the beam stop along the meridian direction was attributed to fibrils. It must be mentioned that the streak scattering is not due to the scattering by voids since the samples are optically transparent excluding any cavities with a size in the range of several hundred nanometers. In addition, if the scattering were due to voiding, the intensity would be much stronger than observed here. The

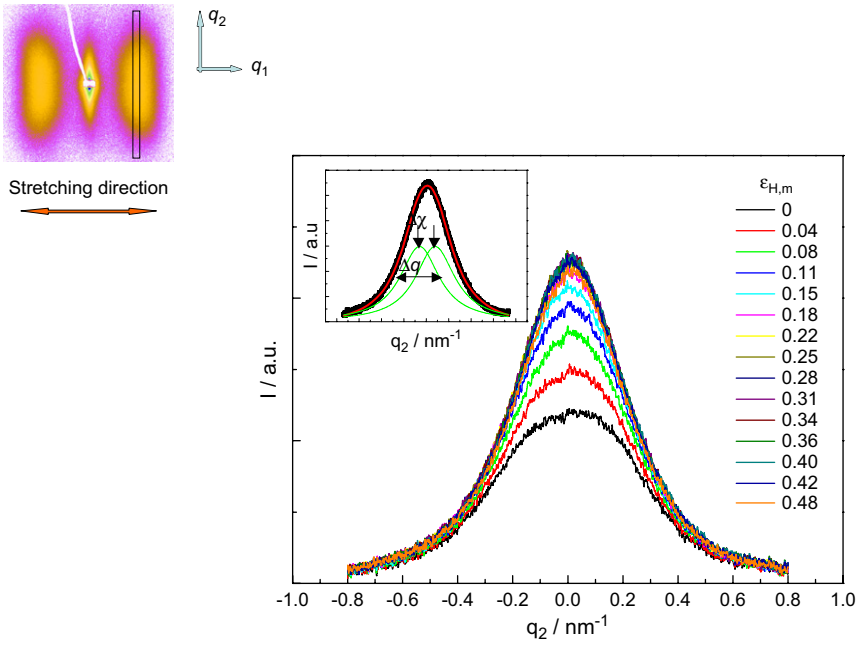

Fig. 5. SAXS: azimuthal scan of the lamellar peaks along q_2 at different macroscopic strains. The inset shows the fit procedure used for the evaluation of the lateral size and the inclination angle of stacks of lamellae.

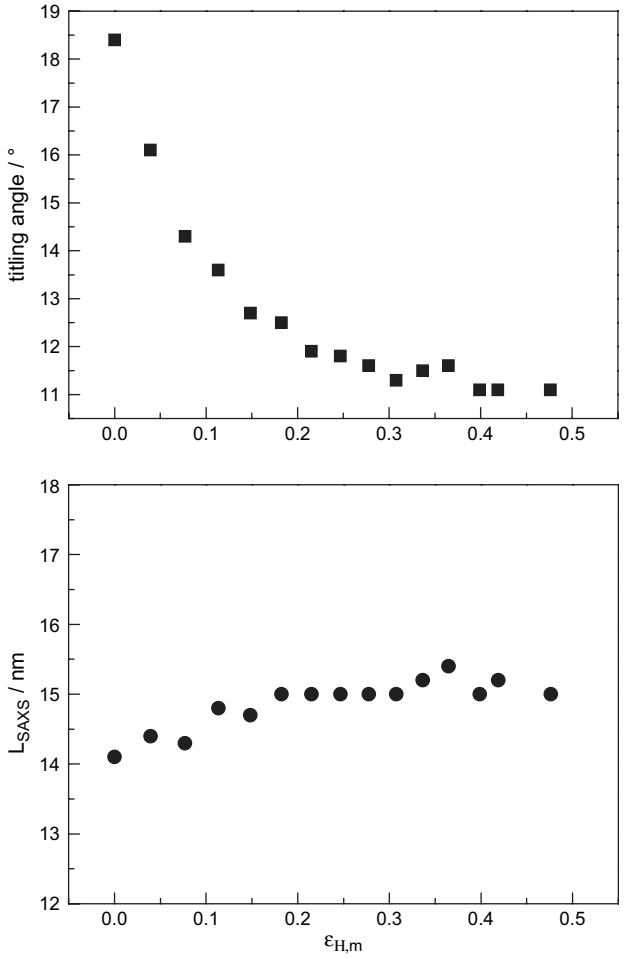

Fig. 6. The tilting angle of lamellar stacks (top) and the lateral size of lamellae (bottom) as function of macroscopic strain.

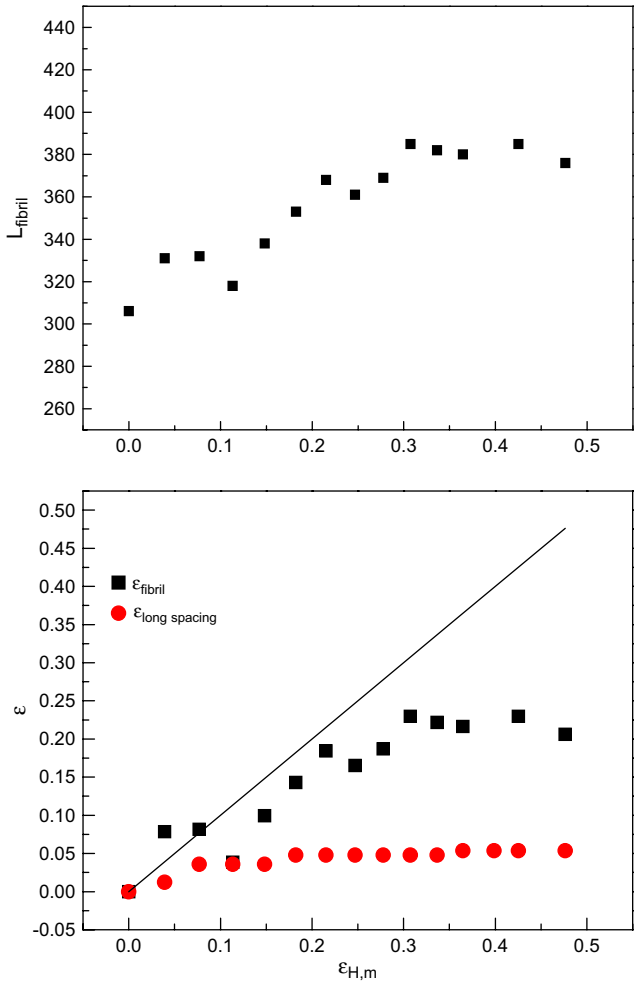

Fig. 7. The length (top) and strain (bottom) of fibrils as a function of the macroscopic strain. For comparison the strain of the lamellar long spacing is also included in the bottom figure. The straight line in the bottom figure represents the affine deformation behavior.

length and misorientation of fibrils can be extracted from the data with the help of the following equation [27]:

$$B_{obs} = \frac{1}{l_f}\frac{2\pi}{q} + B_\Phi \tag{6}$$

where B_{obs} denotes the integral breadth (peak area/peak height), l_f denotes the length of the fibril and B_Φ denotes the misorientation of fibrils. A series of azimuthal scans at different values of scattering vectors q along the meridian were performed and fitted with a Lorentz function. B_{obs} is plotted as a function of $1/q$. The length of the fibrils can be obtained from the slope of the data and the misorientation is given by the intercept.

Results of the average lengths of fibrils as a function of the macroscopic strain are shown in the upper plot of Fig. 7. The length of fibrils is about 300 nm before deformation. It increased to about 390 nm after deformation. The strain of fibrils as a function of macroscopic strain is given in the lower plot of Fig. 7. In the plot, the strain of the crystalline lamellar long spacing as a function of macroscopic strain is also included. The length of fibrils follows roughly affine deformation behavior at small to moderate deformations. Recalling that the strain of the crystalline lamellar long spacing during deformation is almost constant above strains of about 0.07, it is concluded that in between the structural element of stacks of crystalline lamellae and the fibrils there must be another structural element which reacts during the deformation in such a way that both the nearly intact lamellar long spacing and the affine deformation of the fibrils can be accommodated. This structural element can only be the one proposed by Peterlin in his original model for fibres, namely, the micro-fibril.

Considering now the structural aspects of the material being drawn beyond the natural draw ratio we arrive at the following picture: (1) at small elongations up to about 0.15 the amorphous layers between the crystalline lamellae are stretched; (2) during the elongation process non-affine deformation of the local structure sets in at about 0.07, that is, the point where slippage of micro-fibrils passing each other starts resulting in an increase of the length of the fibrils; (3) the resulting affinity of fibril deformation stops at a strain of about 0.3; this arrest is explained by assuming that the slippage of the micro-fibrils is limited since adjacent micro-fibrils are connected by inter-microfibrillar amorphous chains that are increasingly stretched during slippage thus creating

a network of taut polymer chains; (4) further deformation beyond a strain of 0.3 thus finally must be accommodated by the slippage of the fibrils.

The deformation mechanism presented here is different from the deformation mechanism proposed by Peterlin where the slippage of fibrils takes place before micro-fibrils start to slip. The present results indicate that there are stronger interactions between fibrils on a mesoscopic scale than between micro-fibrils on a nanometric scale. The reason for this difference might be the disordered and interlocked arrangement of fibrils, cf. Fig. 2. The fibrils are geometrically well-defined objects as is evidenced from their distinct SAXS-signal. It must be assumed that these objects occur with a distribution of sizes and shapes. The resulting jammed packing makes it more difficult to rearrange the fibrils at low strains compared to local rearrangements of stacks of lamellae in the micro-fibrils they define via their existence.

4. Conclusions

SAXS data on oriented HDPE stretched beyond the natural draw ratio confirm the existence of oriented lamellae, micro-fibrils and fibrils in the system – in line with the structural model proposed by Peterlin. The following sequence of the deformation mechanisms of the deformed oriented HDPE was identified: (1) at small deformations, rubber-like amorphous layers between crystalline lamellae are elongated due to the series arrangement of the lamellae and amorphous layers in the stacks of lamellae in the oriented sample; (2) this elongation of the amorphous layers is limited. At moderate deformations, micro-fibrils made from stacks of crystalline lamellae slip past each other yielding an affine elongation of the fibrils with the macroscopic strain; (3) the slippage of micro-fibrils is arrested at strains of about 0.3 where the slippage of the fibrils sets in. The final step results in a non-affine deformation behavior of the fibrils. The result is different from the mechanism proposed in literature where the slippage of fibrils was believed to occur before the slippage of micro-fibrils.

Acknowledgments

Y.M. thanks the ‘‘Hundred Talents Project’’ of the Chinese Academy of Sciences, the National Basic Research Program of China (2005CB623800), National Natural Science Foundation of China (50603024 and the fund for Creative Research Groups – 50621302) and HASYLAB project II-20052011. We thank R. Döhrmann and M. Dommach for assistance in SAXS experiments at HASYLAB.

References

[1] Hamouda HBH, Simoes-Betbeder M, Grillon F, Blouet P, Billon N, Piques R. Polymer 2001;42:5425.
[2] Huang YL, Brown N. J Polym Sci Part B Polym Phys 1991;29:129.
[3] Rose LJ, Channell CJ, Capaccio G. J Appl Polym Sci 1994;54:2119.
[4] Maier GA, Wallner G, Lang WR, Fratzl P. Macromolecules 2005;38:6099.
[5] Men YF, Rieger J, Enderle HF, Lilge D. Eur Phys J E 2004;15:421.
[6] Yeh JT, Chen JH, Hong HS. J Appl Polym Sci 1994;54:2171.
[7] Wang XQ, Brown N. Polymer 1989;30:1456.
[8] (a) Butler MF, Donald AM. Macromolecules 1998;31:6234;
(b) Chaiyut N, Amornsakchai T, Kaji H, Horii F. Polymer 2006;47:2470.
[9] Peterlin A. J Mater Sci 1971;6:490.
[10] Men YF, Rieger J, Strobl G. Phys Rev Lett 2003;90:095502.
[11] Sadler DM, Barham PJ. Polymer 1990;31:36.
[12] Peterlin A. Colloid Polym Sci 1975;253:809.
[13] Amornsakchai T, Unwin AP, Ward IM, Batchelder DN. Macromolecules 1997;30:5034.
[14] Alt FP, Boehm LL, Enderle HF, Berhold J. Macromol Symp 2001;163:135.
[15] Vinogradov GV, Malkin AY. Rheology of polymer: viscoelasticity and flow of polymers. Springer; 1980.
[16] http://ftp.esrf.fr/pub/expg/FIT2D, 2005.
[17] Murthy NS, Bendarczyk C, Moore RAF, Grubb DT. J Polym Sci Part B Polym Phys 1996;34:821.
[18] Men YF, Rieger J, Lindner P, Enderle HF, Lige D, Kristen MO, et al. J Phys Chem B 2005;109:16650.
[19] Strobl G. The physics of polymers. 2nd ed. Berlin, Germany: Springer; 1997. p. 408.
[20] Strobl GR, Schneider MJ. J Polym Sci Part B Polym Phys 1980;18:1343.
[21] Glatter O, Kratky O. Small-angle X-ray scattering. London, New York: Academic Press; 1982 [chapter 13].
[22] (a) Crist B, Morosoff N. J Polym Sci Part B Polym Phys 1973;11:1023;
(b) Stribeck N, Bayer R, Boesecke P, Camarillo AA. Polymer 2005;46:2579.
[23] Crist B. J Appl Cryst 1979;12:27.
[24] Men YF, Rieger J, Homeyer J. Macromolecules 2004;37:9481.
[25] Guinier A, Fournet G. Small Angle Scattering of X-rays. New York: John Wiley & Sons; 1955 [chapter 2].
[26] Ruland W. J Polym Sci Part C 1969;28:143.
[27] Somani RH, Ling Y, Hiao BS. Macromolecules 2005;38:1244.